Structural modulation and electronic structural features in the charge ordered state of $La_{0.5}Sr_{1.5}MnO_4$

L. J. Zeng, C. Ma, H. X. Yang, R. J. Xiao, and J. Q. Li*
Beijing National Laboratory for Condensed Matter Physics, Institute of Physics, Chinese Academy of Sciences, Beijing 100080, China

J. Jansen
National Centre for HREM, Kavli Institute of Nanoscience, Delft University of Technology, 2628 CJ Lorentzweg 1, Delft, The Netherlands

(Received 28 May 2007; published 16 January 2008)

The structural changes associated with the charge ordering (CO) transition in layered $La_{0.5}Sr_{1.5}MnO_4$ have been determined by electron diffraction using the multislice least-squares method. The results demonstrate that the structural deformations of the $Mn^{3+}O_6$ octahedra can be well characterized by a transverse modulation wave along the ⟨110⟩ direction. Based on these structural data, we have performed a theoretical calculation of the electronic structure by density functional theory plus the on-site Coulomb interaction U. The resultant density of states exhibits a clear band gap at the Fermi level for this low-temperature CO insulating state. It is also noted that the essential Jahn-Teller effects in this layered system can evidently affect the electronic structures and orbital hybridization appearing with the CO transition. Charge disproportionation and orbital ordering in $La_{0.5}Sr_{1.5}MnO_4$ have been extensively discussed in comparison with the data obtained for the cubic perovskite $La_{0.5}Ca_{0.5}MnO_3$.

DOI: 10.1103/PhysRevB.77.024107 PACS number(s): 61.05.J−, 75.47.Lx, 74.25.Jb

INTRODUCTION

Understanding the behaviors of electrons in strongly correlated materials remains a challenging problem. It is believed that the presence of intricate interactions among charge, lattice, spin, and orbital degrees of freedoms is responsible for a variety of the unusual properties discovered in these materials, such as superconductivity and colossal magnetoresistance (CMR). Recent studies also demonstrated that cooperative charge/orbital ordering and electronic phase separation could evidently affect the physical properties in many significant materials, e.g., it sharply suppresses the superconductivity in $La_{2-x}Ba_xCuO_4$ when $x=1/8$,[1,2] and, in particular, can lead to notable structural changes and significantly influence the low-temperature magnetic and transport properties in $(La,Sr)_{n+1}Mn_nO_{3n+1}$ ($n=1$, 2, and ∞) materials.[3–5] The $(La,Sr)_{n+1}Mn_nO_{3n+1}$ materials show a rich variety of physical phenomena that depend quite sensitively on the layered structural features. In the cubic perovskite $La_{1-x}(Sr,Ca)_xMnO_3$, the CMR effect was observed near the ferromagnetic critical temperature, which can be fundamentally interpreted in terms of double-exchange mechanism.[4,6] On the other hand, the "single-layer" solid solution $La_{1-x}Sr_{1+x}MnO_4$ shows strong anisotropic transport properties. Figure 1 shows schematically the structural models of the cubic and layered perovskite phases with $n=\infty$ and 1, respectively. A notable Jahn-Teller (JT) distortion in the layered case is recognizable as an elongation along the c axis. As clearly illustrated in Fig. 1(d), this variation could result in a split of energy levels as discussed in the following context.

The parent compound $La_{1-x}Sr_{1+x}MnO_4$ ($x=0$) shows clear insulating behavior; the hole doping by Sr substitution for La leads to considerable reduction of resistivity in $La_{1-x}Sr_{1+x}MnO_4$, yet all materials with $0.0<x<0.7$ remain insulating or semiconducting. At $x=0.5$, a charge ordering (CO) transition accompanying a steep increase of resistivity occurs at $T_C=220$ K.[7,8] Neutron[9] and x-ray[10] diffraction studies demonstrated a real space order with the alternation of Mn^{3+} and Mn^{4+} sites existing below $T_C=220$ K, and an antiferromagnetic order with a unit cell of $2\sqrt{2}a\times 2\sqrt{2}a\times c$ appears below the Néel temperature of $T_N=110$ K. Moreover, resonant x-ray scattering revealed the presence of orbital ordering and strong cooperative JT distortions of Mn^{3+} ions in the low-temperature CO phase.[11–15] The structural alternation in correlation with CO transitions has been investigated as a significant issue in several typical materials, such as $La_{0.5}Ca_{0.5}MnO_3$, $La_{0.5}Sr_{1.5}MnO_4$, and $LaSr_2Mn_2O_7$,[9,16,17] and certain significant structural features in association with charge/orbital order have been directly observed by *in situ* electron diffraction observations and analyzed based on theoretical calculations.[7,8,16–18] However, accurate atomic displacements associated with the charge/orbital ordering in the layered system have not been determined.[19,20] These structural changes play a critical role for the understanding of low-temperature physical properties in these systems. In this work, we will perform a crystal structure refinement for the structural modulations in $La_{0.5}Sr_{1.5}MnO_4$ using the multislice least-squares (MSLS) method, and we will focus on detailed structural features in the low-temperature CO state to analyze the structural alternations associated with the charge/orbital ordering. Based on the refined structural data, changes of electronic structure along with the CO transition will be extensively discussed. In comparison with the perovskite system $La_{0.5}Ca_{0.5}MnO_3$, the hybridized states of the $d_{z^2-r^2}$ and $d_{x^2-y^2}$ orbitals will be discussed, which could lead to a different orbital ordered state from that in the perovskite material.

EXPERIMENTS AND METHODS

Single-crystalline samples of $La_{0.5}Sr_{1.5}MnO_4$ used in the present study were melt grown by the floating-zone method as reported in previous publications.[3,5] Measurements of transport and magnetic properties revealed a clear CO transition at ~220 K as similarly reported in Refs. 7 and 8.

Transmission electron microscope (TEM) specimens were prepared simply by crushing the $La_{0.5}Sr_{1.5}MnO_4$ material into fine fragments within ethanol, which were then dispersed on a Cu grid coated with a thin carbon film. A Tecnai F20 (200 kV) microscope equipped with a low-temperature sample stage was used to examine structural changes at low temperatures. A DITABIS imaging plates system was used to digitally record the electron diffraction patterns. The average probe size of the electron beam is around 50 nm in diameter. Structure refinements were performed using a recently developed software package MSLS, which performs a standard least-squares refinement in which the measured intensities of the diffracted beams are compared with those calculated using a multislice algorithm. The MSLS refinement can give good results for the light atom positions by using data sets from crystal with different thicknesses. Experimental results showed that the atomic positions obtained by this MSLS procedure are of the same accuracy as those obtained from single-crystal x-ray diffraction.[21]

Electronic structure calculations were carried out by using the full potential linear augmented plane wave method within density functional theory (DFT) in which the exchange and correlation effects were treated by using the local spin density approximation plus U (LSDA+U) via the WIEN2K code.[22] The crystal structure for the CO phase obtained from our structure refinement was used in our calculation for analysis of low-temperature electronic states.

RESULTS

In order to understand the temperature dependence of the crystal structure of $La_{0.5}Sr_{1.5}MnO_4$, we first performed a careful *in situ* TEM examination from 300 K down to 100 K. At room temperature, $La_{0.5}Sr_{1.5}MnO_4$ has a layered perovskite structure with a highly symmetric body-centered tetragonal K_2NiF_4 structure with the space group of $I4/mmm$ [a =3.86(1) Å, c=12.42(2) Å], this layered material has a notable pseudo two-dimensional character and strongly anisotropic transport properties. Figures 1(a)–1(d) show certain critical structural features of $La_{1-x}Sr_{1+x}MnO_4$ in comparison with the cubic perovskite phase of $La_{1-x}(Sr,Ca)_xMnO_3$. In the cubic phase, the strong Hund's rule coupling and the large cubic (O_h) component of the crystal field allow the 3d orbitals to split into the two degenerate levels of t_{2g} and e_g; the Mn^{3+} ($3d^4$) site therefore has three valence electrons in t_{2g} and one valence electron in the twofold degenerate e_g level. In contrast, the degeneracy of the e_g level can be further lifted by the JT distortions of the MnO_6 octahedra in the layered system as shown in Figs. 1(d) and 1(f). Hence, it is expected that this notable difference in crystal field splitting of the 3d orbitals should result in certain specific features in the low-temperature charge ordered states of the layered system.

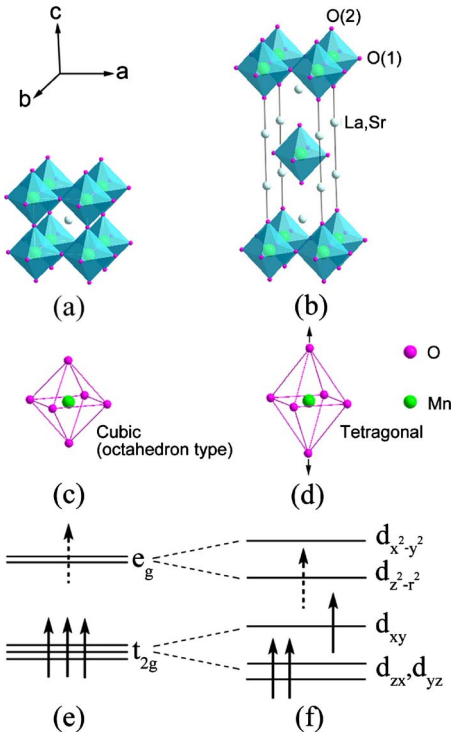

FIG. 1. (Color online) Schematic diagrams for the structures of $(La,Sr)_{n+1}Mn_nO_{3n+1}$ with n=(a) ∞ and (b) 1. (c) An octahedron in the cubic perovskite phase. (d) A Jahn-Teller distorted octahedron in $La_{1-x}Sr_{1+x}MnO_4$. Also shown are the crystal-field splitting of the 3d band orbitals (e) in the cubic and (f) in the layered phase.

Figures 2(a)–2(d) show the [001] and [1$\bar{1}$0] zone-axis electron diffraction patterns obtained, respectively, at temperatures of 300 and 100 K for $La_{0.5}Sr_{1.5}MnO_4$, illustrating the evident structural change at the CO transition associated with T_C~220 K. The most striking feature is the appearance of sharp superlattice spots in the [001] zone-axis pattern taken below T_C. The observed fourfold superlattice spots in the electron diffraction patterns in general appear at commensurate positions with a modulation wave vector of q =(1/4,1/4,0) along the a^*+b^* direction, where a^* and b^* are the reciprocal lattice vectors for the basic tetragonal structure. It is also noted that this modulation becomes completely invisible as the sample tilted to the [1$\bar{1}$0] zone-axis direction as shown in Fig. 2(d). These facts suggest that the structural distortion in this CO state can be well described as a displacement-type modulation corresponding to a polarization of the MnO_6 octahedra along the ⟨1$\bar{1}$0⟩ axis direction, i.e., the CO modulation in the present case produces a transverse wave at low temperatures. Therefore, in the following discussion we will mainly focus on the observations along the c axis direction to reveal the structure changes. Actually, the structural and magnetic alternations associated with the charge/orbital ordering in manganites were considered as important issues in previous studies. The observations of two independent magnetic sublattices by neutron powder diffraction were interpreted as a charge disproportionation between two typical Mn sites; moreover, the appearance of new Bragg reflections in the diffraction pattern was interpreted by

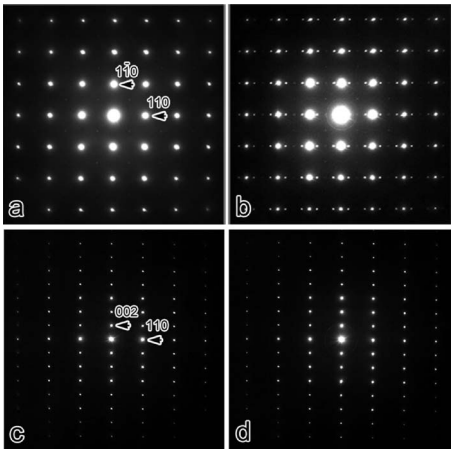

FIG. 2. The [001] zone-axis electron diffraction patterns of $La_{0.5}Sr_{1.5}MnO_4$ obtained respectively at (a) 300 and (b) 100 K. The presence of superlattice reflections at low temperature is evident. The fundamental spots were indexed on the basis of the tetragonal unit cell. Also shown are the $[1\bar{1}0]$ zone-axis electron diffraction patterns of $La_{0.5}Sr_{1.5}MnO_4$ obtained at (c) 300 and (d) 100 K, respectively. No superlattice reflections were observed in (d), suggesting a transverse wave for structural modulation with the polarization along the $\langle 1\bar{1}0\rangle$ direction. (In this paper, the planes and directions are all indexed based on the room-temperature tetragonal unit cell if not noted specially.)

the cooperative magnetic ordering corresponding with an antiferromagnetic structure with $T_N \sim 110$ K.[9]

In this section we will analyze the fundamental structural features of the low-temperature structure associated with the charge/orbital ordering transition. According to the results of our *in situ* TEM observations and previous experimental results on the related materials,[16,17,23,24] we propose a structural model for the low-temperature superstructure. This superstructure is considered to be a supercell with $a_s \approx c$, $b_s \approx a-b$, and $c_s \approx 2a+2b$, where a, b, and c are the basic lattice vectors of the tetragonal structure, and a_s, b_s, and c_s are the lattice vectors of the supercell for the CO phase. This supercell has an orthorhombic structure with the space group of *Cmcm*, and has dimensions of $\sqrt{2}a \times 2\sqrt{2}a \times c$ relative to the tetragonal cell, showing similar features in comparison with the models proposed for other related charge ordered phases, e.g., $La_{0.5}Ca_{0.5}MnO_3$ (Ref. 23) and the bilayered $LaSr_2Mn_2O_7$.[24] On the other hand, this model is different from the model in Ref. 9 in which no orbital order is considered. Figure 3(b) illustrates a structural model exhibiting the atomic displacements projected along the a_s axis direction (i.e., c axis direction in the tetragonal structure); the structural model at room temperature is also shown in Fig. 3(a) for comparison. In this superstructure model, the Mn, La(Sr), and O atoms are distributed on eight sites; the two typical Mn sites are denoted as Mn(1) and Mn(2), as listed in Table I. According to the experimental structural data for the CO state obtained in other related manganese systems,[23,24] the major structural distortions in general appear in the $Mn^{3+}O_6$ octahedra, arising essentially from the e_g orbital electrons. Therefore, in order to get better results in the following structure refinements, we can also introduce certain constraints on the structural distortion for $La_{0.5}Sr_{1.5}MnO_4$ within the *Cmcm* symmetry: (1) the four O atoms in the b_s-c_s plane surrounding the Mn(2) sites (i.e., Mn^{4+} ions) were jointly shifted following the Mn(2) atoms, resulting a roughly undistorted octahedron with Mn-O distances of about 1.930 Å; (2) the $Mn(2)O_6$ octahedron centered at $(0,1/2,1/4)$ was shifted along the b_s axis toward the Mn(1) atoms at (0,1,0) and $(0,1,1/2)$ by Δy, while the $Mn(2)O_6$

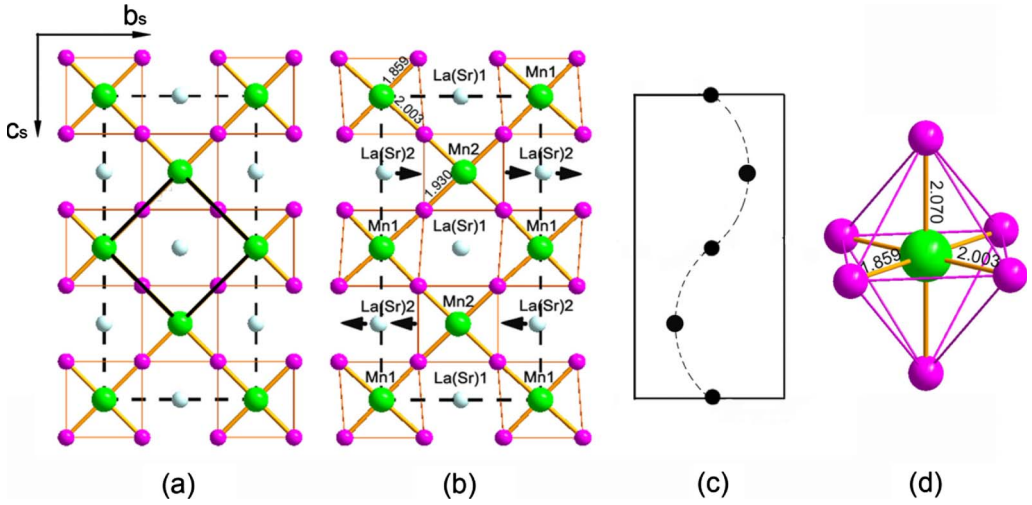

FIG. 3. (Color online) Schematic structural models of $La_{0.5}Sr_{1.5}MnO_4$ projected on the b_s-c_s plane (i.e., a-b plane in the tetragonal structure). (a) Room temperature structure of $La_{0.5}Sr_{1.5}MnO_4$. b_s and c_s axis directions of supercell are indicated. The black thick lines show the unit cell of the room-temperature $I4/mmm$ structure, while the dashed lines show the low-temperature supercell with dimensions of $\sqrt{2}a \times 2\sqrt{2}a \times c$. (b) Low-temperature structure of $La_{0.5}Sr_{1.5}MnO_4$; arrows indicate the displacements of the $Mn(2)O_6$ octahedra (Δy) and of the La(Sr)(2) atoms. The oxygen atoms are not labeled. The La(Sr) atoms are on the sites below the Mn-O plane (see Fig. 1). (c) Sketch of the refined atomic displacements in association with charge ordering. (d) The deformed $Mn^{3+}O_6$ octahedron in the low-temperature structure, in which the different Mn-O bond lengths in three directions are shown.

TABLE I. Atomic positions and occupancies for $La_{0.5}Sr_{1.5}MnO_4$ for the low-temperature superstructure, based on a fourfold cell with *Cmcm* symmetry. Mn(2) atoms are at positions $(0,y,1/4)$; O(1) and O(4) are at positions of $(0,y,z)$, and La(Sr)(2) are at positions $(x,y,1/4)$. The MSLS method yields $\Delta y=0.018\,71(1)$. The numbers shown in the second column indicate the site multiplicity.

Atom	Multiplicity	x	y	z	B (Å^2)	Occupancy
Mn(1)	×4	0.0	0.0	0.0	0.26(3)	1.0
Mn(2)	×4	0.0	$0.5-\Delta y$	0.25	0.25(1)	1.0
O(1)	×8	0.0	$0.25-\Delta y$	0.125	1.10(1)	1.0
O(2)	×8	0.3333	0.5	0.0	0.90(2)	1.0
O(3)	×8	0.1666	$0.5-\Delta y$	0.25	1.00(4)	1.0
O(4)	×8	0.0	$0.75-\Delta y$	0.125	0.99(3)	1.0
La(1)	×8	0.8333	0.5	0.0	0.60(2)	0.25
La(2)	×8	0.1666	$0.0-\Delta y$	0.25	0.60(2)	0.25
Sr(1)	×8	0.8333	0.5	0.0	0.61(2)	0.75
Sr(2)	×8	0.1666	$0.0-\Delta y$	0.25	0.61(2)	0.75

octahedron centered at $(0,1/2,3/4)$ was shifted in the opposite direction (see Table I); (3) the La(Sr) atoms were shifted by Δy in the same direction following the neighboring $Mn(2)O_6$ octahedra; (4) the Mn(1) and other La(Sr) and O atoms were left undisturbed.

Table II shows the electron diffraction data used for the structural refinements by using the MSLS program.[21] The R value used in our refinement is defined as $R(I^2)=\Sigma[(I_{obs})-(I_{calc})]^2/\Sigma(I_{obs})^2$, using only the significant reflections with $I_{obs}>2\sigma(I_{obs})$ [$\sigma(I_{obs})$ is the standard deviation of the intensity]. Diffraction patterns for the present analysis were obtained by using an incident electron beam with only a small convergence angle, such that the illumination is similar to a plane wave, resulting in sharp diffraction spots; the intensity of each reflection was measured by integrating over a surrounding circular area in the diffraction pattern. A small spot size for electron diffraction was used in order to have a relatively small variation of thickness and crystal orientation, since most crystals are wedge shaped, and to reduce the amount of unwanted information about, e.g., impurities and defect structures. First, the scale factor, crystal misorientation, and thickness for each electron diffraction pattern were refined. Four sets of experimental data were then selected and all subsequent refinements were done simultaneously on those sets. Data for each electron diffraction pattern are separately listed in Table II. The overall R value of all four sets of data is 3.9%. Detailed refinement results can be found in Tables I and II. The resultant structural data are given as $\Delta y=0.018\,71(1)$, and the $Mn(1)^{3+}O_6$ octahedra have notable structural distortion recognizable as two different Mn-O bond lengths in the b_s-c_s plane, as shown in Figs. 3(b) and 3(d), i.e., about 2.003 and 1.859 Å. Figure 3(c) shows the modulation wave for atomic displacements. The bond deformation for the $Mn(1)^{3+}O_6$ octahedra has a simple sinusoidal behavior within the b_s-c_s basal plane. Figure 3(d) illustrates the deformed $Mn(1)O_6$ octahedron in the CO state, clearly showing the Mn-O distances along three different directions. Our following theoretical study demonstrates that these structural changes are essentially in correlation with the low-temperature charge/orbital ordering, which eventually results in notable changes in electronic structure.

Based on the above refined structure, we have further performed a theoretical study on the change of electronic structure across the phase transition. The density of states and charge density contours were calculated by using the full potential linear augmented plane wave method within density functional theory in which the exchange and correlation effects were treated by using the local spin density approximation plus U via the WIEN2K code.[22] The muffin-tin radii R_{MT} were selected as 2.1 a.u. for La and Sr atoms, 2.0 a.u. for Mn atoms, and 1.5 a.u. for O atoms. The maximum angular momentum of the radial wave functions (l_{max}) was chosen as 10 and $R_{MT}K_{max}$ was fixed at 6.0 to determine the basis size. The doping effect in $La_{0.5}Sr_{1.5}MnO_4$ is treated by constructing a $2\times2\times1$ supercell with 112 atoms, and the k-point mesh used is $3\times2\times3$ for this supercell. The ferromagnetic ordering was considered. It is known that the on-site Coulomb interaction U can evidently affect electronic structural features of strongly correlated systems. We here will mainly discuss the results obtained for $U=5$ eV, as used in other related materials.[25] Figure 4 shows the projected density of states onto Mn(1) 3d and Mn(2) 3d orbitals. The most striking feature shown in this figure is the notable difference of occupations for electronic states on Mn(1) and Mn(2) sites, which directly demonstrates the presence of

TABLE II. Experimental data of electron diffraction used for the structure refinement [using only the reflections $I_{obs}>2\sigma(I_{obs})$]. The shown electron diffraction patterns are indexed based on the supercell with space group of *Cmcm*. In the present work, we use the data taken from four crystal areas with different thicknesses. The misorientation of the crystal is given as the center of the Laue circle in the electron diffraction pattern in Miller indices h, k, and l as illustrated for each pattern.

Zone axis	Number of observed reflections	Thickness (nm)	Crystal misorientations (center of Laue circle)			R value (%)
			h	k	l	
$[100]_s$	217	3.17(2)	0	−1.03(2)	−2.4(4)	5.1
$[100]_s$	154	10.9(2)	0	0.13(2)	0.38(1)	3.6
$[100]_s$	192	7.98(1)	0	−0.9(1)	0.14(3)	3.3
$[100]_s$	82	9.80(1)	0	0.23(3)	0.11(2)	2.1

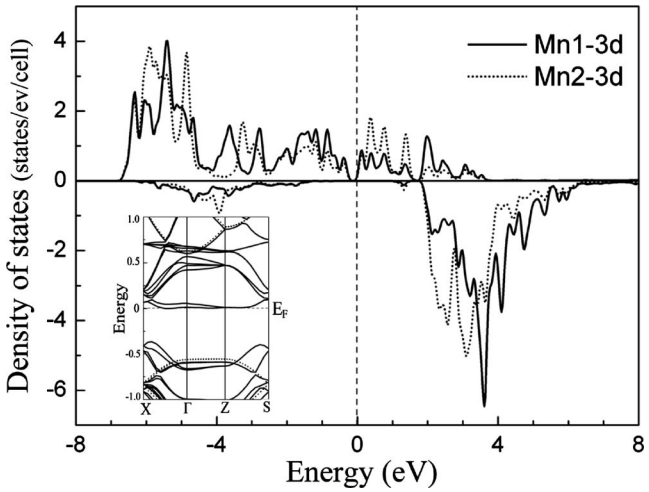

FIG. 4. Density of states projected onto the Mn(1) $3d$ (solid line) and Mn(2) $3d$ (dotted line) orbitals calculated by the LSDA $+U$ with $U=5$ eV. The dashed line marks the Fermi energy. The remarkable difference in the charge density on the Mn(1) and Mn(2) sites is illustrated. The inset is the electronic band structure for the CO phase, where the solid and dashed lines denote spin up and down, respectively.

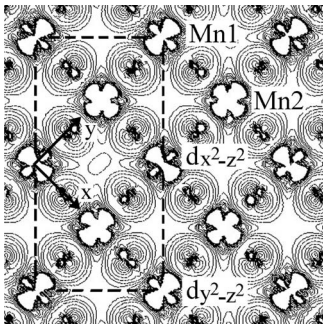

FIG. 5. Valence charge density contour plotted on the basal plane of $La_{0.5}Sr_{1.5}MnO_4$. The solid lines denote the isodensity curves. The dashed line shows the unit cell used in our calculations.

charge disproportionation in $La_{0.5}Sr_{1.5}MnO_4$ at low temperatures. Careful analysis reveals that the electronic states near the Fermi surface mainly arise from the Mn $3d$ hybridized with the O $2p$ states, and an energy gap of about 0.35 eV, but 0.02 eV at 300 K,[28] apparently exists at the Fermi level as shown in the band structure in the inset of Fig. 4. This fact suggests an insulating behavior in the CO state in good agreement with the measurements of transport properties.[7] The calculated difference between the charge density on the nominal $Mn(1)^{3+}$ and $Mn(2)^{4+}$ sites is about 0.1 electrons through integrating the occupied states in the density of states, which is comparable with the data obtained theoretically in the $La_{0.5}Ca_{0.5}MnO_3$ system.[25,26] However, the DFT calculation usually underestimates charge disproportionation as described in Ref. 25. Actually, owing to the remarkable structural distortion and the oxygen displacements in the $Mn^{3+}O_6$ octahedra, hybridization of the $d_{z^2-r^2}$ and $d_{x^2-y^2}$ orbitals occurs following the CO transition, and the $3d$ electrons in the e_g level are redistributed among certain degenerate orbitals. As a result, a visible orbital ordered state is reached at low temperature in association with the alternations in both the structure and the charge density. Figure 5 shows a contour map illustrating the valence charge density for the CO phase, directly showing the charge and orbital ordering on the basal plane. The $3d$ electrons on the $Mn(1)^{3+}$ sites first occupy three t_{2g} up-spin orbitals (d_{xy}, d_{xz}, d_{yz}), followed by the other electrons occupying hybridized states of the $d_{z^2-r^2}$ and $d_{x^2-y^2}$ orbitals, depending on the structural distortion. Our careful analysis of the calculated data for this layered system suggests this state can be characterized as $d_{x^2-z^2}$ or $d_{y^2-z^2}$ as recognizable in Fig. 5. It is worthwhile to point out that this kind of orbital ordered state is quite different from what was observed in the cubic $La_{0.5}Ca_{0.5}MnO_3$ perovskite,[25] in which the $d_{3x^2-r^2}$ and $d_{3y^2-r^2}$ orbitals are ordered in a d_{z^2}-type zigzag pattern within the a-b plane. Hence, it is impossible to simply interpret the orbital ordering in the layered systems by the known d_{z^2} zigzag chain picture[27] as commonly used in the cubic $La(Ca,Sr)MnO_3$ materials. A further study of the electronic structure features, in particular the orbital hybridization, within the charge/orbital ordered state in layered $(La,Sr)_{n+1}Mn_nO_{3n+1}$ with $n=1$ and 2, is still in progress.[28]

CONCLUSIONS

In summary, *in situ* TEM observations reveal a clear structural phase transition related to the charge/orbital order in $La_{0.5}Sr_{1.5}MnO_4$ at the critical temperature of $T_C=220$ K. Structural distortion in this layered system can be well described by a displacement-type modulation resulting in a transverse wave in the CO state. The structure refinement using the multislice least-squares method demonstrates that the Mn atoms, at symmetry-equivalent sites at room temperature, are distributed at two crystallographically inequivalent sites in the low-temperature CO phase. The results also show that the structural deformations of the $Mn^{3+}O_6$ octahedra can be well characterized by a transverse modulation wave moving along the ⟨110⟩ directions. Based on these structure data, first-principles calculation reveals certain notable features in electronic structures: the density of states exhibits a clear band gap of ~0.3 eV at the Fermi level for the low-temperature CO insulating state; charge disproportionation and orbital ordering are evidently visible in the contour map of valence charge density. In particular, the $d_{x^2-z^2}$ or $d_{y^2-z^2}$ orbital ordering is well demonstrated for this layered material, which is rather different from the d_{z^2} zigzag pattern observed in cubic $La_{0.5}Ca_{0.5}MnO_3$ perovskite. Hence, our results demonstrate that the layered structural features have a notable influence on the local structural distortion, electronic structure properties, and low-temperature orbital ordering in these manganese materials.

ACKNOWLEDGMENTS

We would like to thank D. Van Dyck for fruitful discussions. The work reported here iss supported by the National Natural Science Foundation of China, Chinese Academy of Sciences (KJCX2-YW-M04), and the Ministry of Science and Technology of China.

*Corresponding author. LJQ@aphy.iphy.ac.cn

[1] A. R. Moodenbaugh, Y. Xu, M. Suenaga, T. J. Folkerts, and R. N. Shelton, Phys. Rev. B **38**, 4596 (1988).
[2] T. Valla, A. V. Fedorov, Jinho Lee, J. C. Davis, and G. D. Gu, Science **314**, 1914 (2006).
[3] Y. Moritomo, A. Asamitsu, H. Kuwahara, and Y. Tokura, Nature (London) **380**, 141 (1996).
[4] A. Urushibara, Y. Moritomo, T. Arima, A. Asamitsu, G. Kido, and Y. Tokura, Phys. Rev. B **51**, 14103 (1995).
[5] T. Kimura, Y. Tomioka, H. Kuwadara, A. Asamitsu, M. Tamura, and Y. Tokura, Science **274**, 1698 (1996).
[6] J. B. Goodenough, Phys. Rev. **100**, 564 (1955).
[7] Y. Moritomo, Y. Tomioka, A. Asamitsu, and Y. Tokura, Phys. Rev. B **51**, 3297 (1995).
[8] Wei Bao, C. H. Chen, S. A. Carter, and S.-W. Cheong, Solid State Commun. **98**, 55 (1996).
[9] B. J. Sternlieb, J. P. Hill, U. C. Wildgruber, G. M. Luke, B. Nachumi, Y. Moritomo, and Y. Tokura, Phys. Rev. Lett. **76**, 2169 (1996).
[10] Y. Murakami, H. Kawada, H. Kawata, M. Tanaka, T. Arima, Y. Moritomo, and Y. Tokura, Phys. Rev. Lett. **80**, 1932 (1998).
[11] S. B. Wilkins, P. D. Spence, P. D. Hatton, S. P. Collins, M. D. Roper, D. Prabhakaran, and A. T. Boothroyd, Phys. Rev. Lett. **91**, 167205 (2003).
[12] S. B. Wilkins, N. Stojic, T. A. Beale, N. Binggeli, C. W. M. Castleton, P. Bencok, D. Prabhakaran, A. T. Boothroyd, P. D. Hatton, and M. Altarelli, Phys. Rev. B **71**, 245102 (2005).
[13] U. Staub, V. Scagnoli, A. M. Mulders, M. Janousch, Z. Honda, and J. M. Tonnerre, Europhys. Lett. **76**, 926 (2006).
[14] A. Mirone, S. S. Dhesi, and G. Van der Laan, Eur. Phys. J. B **53**, 23 (2006).
[15] S. S. Dhesi, A. Mirone, C. De Nadaï, P. Ohresser, P. Bencok, N. B. Brookes, P. Reutler, A. Revcolevschi, A. Tagliaferri, O. Toulemonde, and G. van der Laan, Phys. Rev. Lett. **92**, 056403 (2004).
[16] C. H. Chen and S.-W. Cheong, Phys. Rev. Lett. **76**, 4042 (1996).
[17] J. Q. Li, Y. Matsui, T. Kimura, and Y. Tokura, Phys. Rev. B **57**, R3205 (1998).
[18] Priya Mahadevan, K. Terakura, and Sarma, Phys. Rev. Lett. **87**, 066404 (2001).
[19] S. Larochelle, A. Mehta, L. Lu, P. K. Mang, O. P. Vajk, N. Kaneko, J. W. Lynn, L. Zhou, and M. Greven, Phys. Rev. B **71**, 024435 (2005).
[20] D. Senff, P. Reutler, M. Braden, O. Friedt, D. Bruns, A. Cousson, F. Bourée, M. Merz, B. Büchner, and A. Revcolevschi, Phys. Rev. B **71**, 024425 (2005).
[21] J. Jansen, D. Tang, H. W. Zandbergen, and H. Schenk, Acta Crystallogr., Sect. A: Found. Crystallogr. **54**, 91 (1998).
[22] P. Blaha, K. Schwarz, G. Madsen, D. Kvasnicka, and J. Luitz, computer code WIEN2K (Karlheinz Schwarz Technical University, Wien, Austria).
[23] P. G. Radaelli, D. E. Cox, M. Marezio, and S.-W. Cheong, Phys. Rev. B **55**, 3015 (1997).
[24] D. N. Argyriou, H. N. Bordallo, B. J. Cambell, A. K. Cheetham, D. E. Cox, J. S. Gardner, K. Hanif, A. dos Santos, and G. F. Strouse, Phys. Rev. B **61**, 15269 (2000).
[25] Z. Popović and S. Satpathy, Phys. Rev. Lett. **88**, 197201 (2002).
[26] V. Ferrari, M. Towler, and P. B. Littlewood, Phys. Rev. Lett. **91**, 227202 (2003).
[27] I. V. Solovyev and K. Terakura, Phys. Rev. Lett. **83**, 2825 (1999).
[28] C. Ma and J. Q. Li (unpublished).